Deformation Monitoring and Analysis of Railway Bridges Integrating Time-Series InSAR and Finite-Element Modeling

Xiaoqiong Qin [1,2], Qingbo Ma [1,2], Chisheng Wang [3 *], Linfu Xie [3], Xiangsheng Chen [1,2]

[1] State Key Laboratory of Intelligent Geotechnics and Tunnelling, Shenzhen University, Shenzhen, 518060, China
[2] School of Civil and Traffic Engineering & Underground Polis Academy, Shenzhen University, Shenzhen, 518060, China
[3] Smart City Research Institute & School of Architecture and Urban Planning, Shenzhen University, 518060, China

Keywords: Railway Bridge, InSAR, FEM, Deformation, Thermal Effects.

Abstract

Interferometric Synthetic Aperture Radar (InSAR) is widely employed for measuring millimetre-level deformation of bridges and other structures. However, retrieving multi-dimensional displacements of a bridge and integrating these measurements with structural stress for coupled analysis remains a major challenge. To address this issue, we propose an integrated framework and demonstrate its application to the Hutiaohe extra-large bridge in Guizhou Province. First, a two-dimensional E-PS-InSAR time-series method is developed to derive the bi-directional deformation of the bridge. Next, structural temperatures are obtained via the ANUSPLIN interpolation scheme, enabling accurate isolation of the thermal response. Finally, the finite-element model (FEM) of the bridge is established to interpret the observed deformation and thermal signatures within the structural context. The results indicate that, compared to conventional InSAR approaches, the proposed framework provides a richer set of insights of multi-dimensional deformation, structural behavior, and thermal effects.

1. Introduction

By the end of 2023, China’s high-speed railway network has been extended to 45,000 km, with more than half of this length constructed on bridge structures. On certain corridors, such as the Beijing–Shanghai line, the proportion of bridges exceeded 85% (Su et al., 2022). Given this expanding inventory and increasing proportion, large-area and high-precision operational monitoring of railway bridges became a critical issue for infrastructure authorities. Benefiting from all-day, all-weather, high-resolution and millimetre-level accuracy, Space-borne Interferometric Synthetic Aperture Radar (InSAR) developed rapidly and has been extensively applied to deformation monitoring of urban structures (Liao et al., 2020; Qin et al., 2021; Cai et al., 2022; Xiao et al., 2022; Shi et al., 2019). Nevertheless, a review of the current literature indicates that most studies merely estimate displacements without further investigating the structural response (Selvakumaran et al., 2020; Schlögl et al., 2021; Alani et al., 2020; Xiong et al., 2021).

From the perspective of bridge monitoring, some studies have combined InSAR data with finite element model (FEM) simulation to analyze the correlation between surface deformation and internal structural stress of long-span railway bridges (Zhang et al., 2023; Wang et al., 2024). However, most of these studies are carried out in regions with relatively stable geological conditions, and their adaptability to complex geological environments still needs to be further verified.

This study focused on railway bridges, utilizing E-PS-InSAR to retrieve the structural three-dimensional displacements. Then, a high-fidelity finite-element model was constructed to investigate the deformation mechanism of the bridge. Through the integration of the deformation measurements obtained from InSAR and the insights derived from the finite-element model, the study unravelled the complex coupling between deformation mechanisms and structural responses, with particular attention paid to thermal effects. The findings of this research offer a robust foundation for comprehending the deformation behavior and identifying potential instability factors in high-speed railway bridges and similar structural types.

2. Study Area and Datasets

2.1 Study Area

The Hutiaohe Extra-Large Bridge, located at Liupanshui Municipality, Guizhou Province, is a simply-supported multi-track railway bridge (Fig 1). Situated on the Yunnan–Guizhou Plateau, the bridge lies within a subtropical monsoon climatic zone that is characterised by rugged topography and frequent weather fluctuations. Large diurnal temperature differences and an annual temperature amplitude of approximately 30 ℃ make the area an ideal natural laboratory for investigating the deformation behaviour of railway bridges in mountainous regions.

The bridge is 1,108.4 m long and comprises 89 piers arranged at 33 pier positions as shown in Fig. 2(a). Among these positions, 23 are three-bearing and 10 are two-bearing configurations. For analytical convenience, the pier positions were numbered from west to east as #1 to #33. The central span at each position is 32.6 m. A high-speed railway station—Pu’anxian Station—is constructed on the deck between Pier #2 and Pier #16.

* Corresponding author

This contribution has been peer-reviewed. The double-blind peer-review was conducted on the basis of the full paper.
https://doi.org/10.5194/isprs-annals-XI-3-2026-455-2026 | © Author(s) 2026. CC BY 4.0 License.

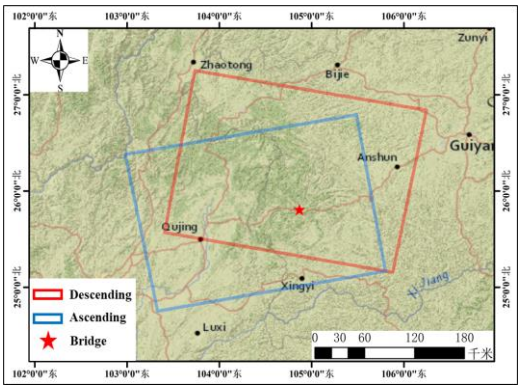

Fig 1. Bridge Location and Image Coverage

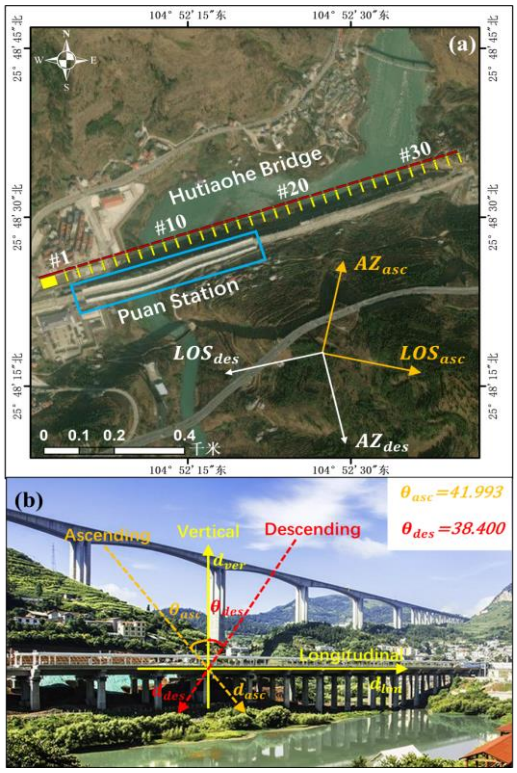

Fig 2. Bridge overview: (a) schematic of the bridge; (b) satellite incidence angle

2.2 Datasets

This study collected C-band Sentinel-1 images covering the target bridge, consisting of 32 descending scenes acquired from December 2017 to January 2020 and 32 ascending scenes from December 2017 to January 2020. The spatial coverage is shown in Fig. 1, and the look angle is illustrated in Fig. 2(b). The Spatial-temporal baseline distribution is provided in Fig 3.

To characterize the thermal response of the bridge, this study employed the NOAA Global Station Daily Meteorological Indicators dataset spanning 1929–2024. The archive comprises 12 variables—including mean temperature, mean dew-point, mean sea-level pressure and mean visibility—and is distributed by the National Centers for Environmental Information of the U.S. National Oceanic and Atmospheric Administration.

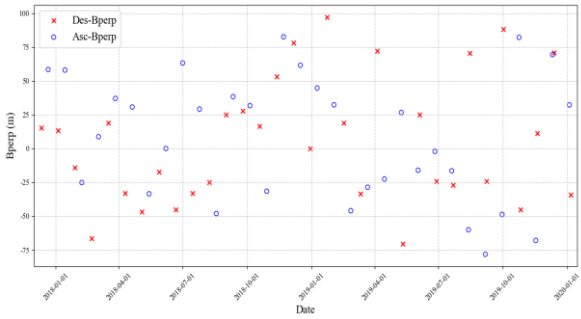

Fig 3. Spatial-temporal baselines of the SAR images.

3. Methodology

This study proposed an integrated framework that jointly exploits ascending- and descending-track TS-InSAR together with finite-element (FEM) analysis. The framework consists of three core components: (i) a 2-D deformation time-series eatimation based on E-PS-InSAR, (ii) high-precision extraction of bridge-specific thermal effects via the ANUSPLIN interpolation scheme, and (iii) deformation interpretation supported by a FEM of the bridge. The overall research workflow is illustrated in Fig. 4.

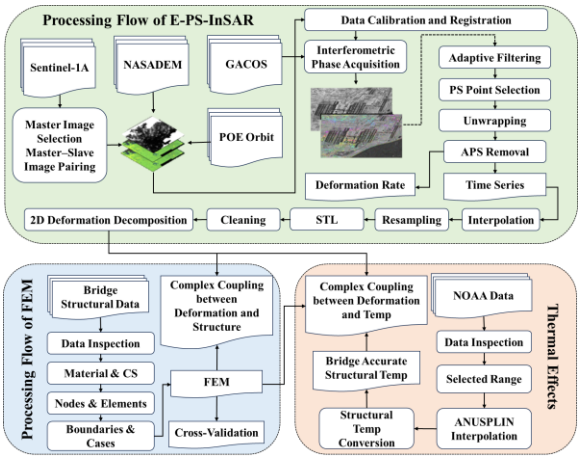

Fig 4. Research Roadmap

4. Experimental Results and Analysis

4.1 The LOS Deformation

Fig. 5 presents the LOS deformation rates of the Hutiaohe Bridge, where the 5(a) and 5(b) are derived from the ascending and descending data of the Sentinel-1, respectively. The measurement points (MPs) of the bridge, derived from both ascending and descending data, are evenly distributed. Moreover, the deformation of the bridge is small, ranging between -3 mm/a and 3 mm/a. As a high-speed railway simply-supported bridge, it has higher construction standards, smaller span, and lower deck height than regular road bridges, enhancing structural stability and minimizing deformation.

This contribution has been peer-reviewed. The double-blind peer-review was conducted on the basis of the full paper.
https://doi.org/10.5194/isprs-annals-XI-3-2026-455-2026 | © Author(s) 2026. CC BY 4.0 License.

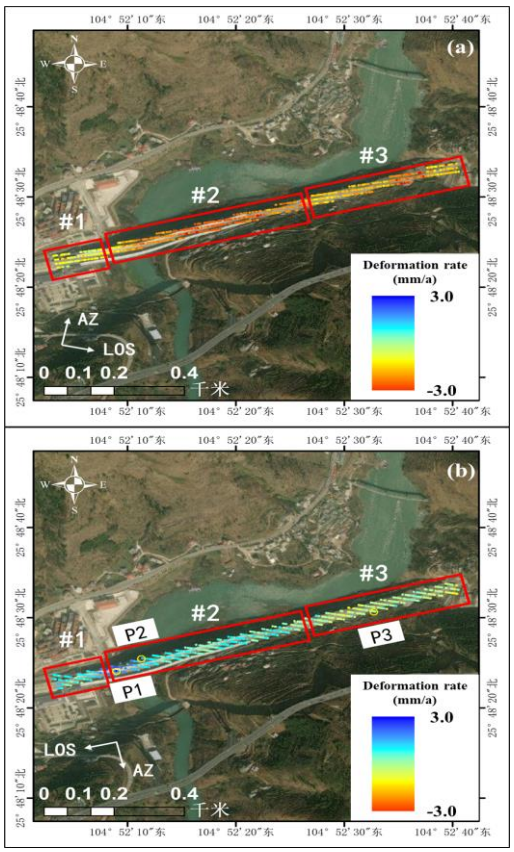

Fig 5. LOS deformation rates of Hutiaohe bridge: (a) The Ascending Sentinel-1; (b) The Descending Sentinel-1

The MPs on the bridge deck can be categorized into three sections: #1, #2, and #3. From ascending data, the LOS deformation rates of the target bridge range from -3 mm/a to 0.5 mm/a. The maximum subsidence is at section #2, and the maximum uplift is at #3. From descending data, the LOS deformation rates are between -1.8 mm/a and 3 mm/a. The maximum uplift is at #2, and the maximum subsidence is at #3. The ascending and descending results show opposite trends. This may be due to the opposite look angles of the satellites in ascending and descending tracks. The deformation time-series were further processed through temporal interpolation, resampling, STL decomposition and outlier cleaning to eliminate unreasonable values by means of the 3-sigma rule. The procedure removed outliers, filled data gaps and produced smoothly interpolated series, providing a robust basis for subsequent time-series analyses.

4.2 Thermal Effects

Based on daily meteorological indicator data from Chinese observational stations spanning 1942–2024, this study selected an interpolation domain of approximately 150,000 km ²and generated day-by-day temperature fields for the bridge by means of the ANUSPLIN trivariate spline model. The interpolated result is displayed in Fig. 6: the green curve denotes the in-situ measured ambient air temperature, the blue curve gives the refined ambient temperature at the bridge location, and the red curve represents the derived structural temperature of the bridge.

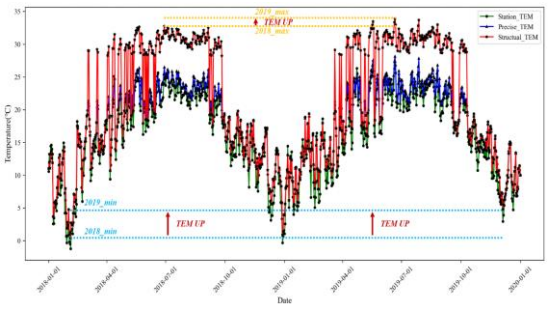

Fig 6. Temperature Interpolation Results

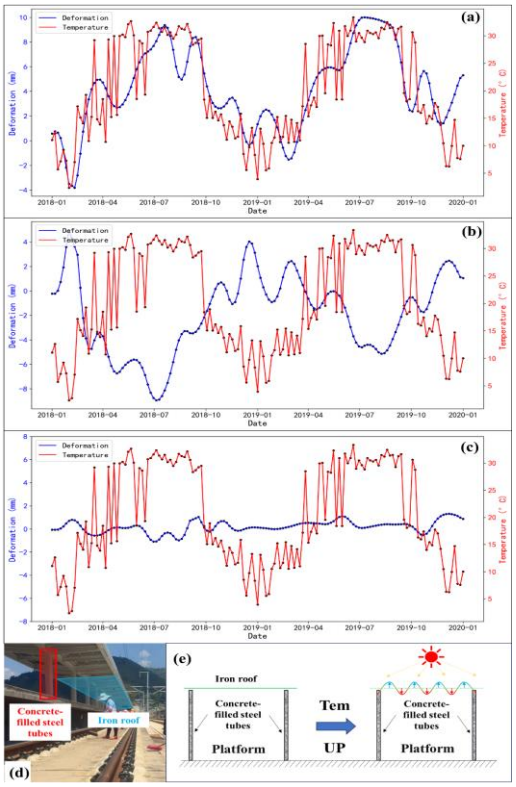

Fig 7. Three representative time-series curves: (a) positive correlation; (b) negative correlation; (c) no correlation; (d) & (e) schematic diagrams

Three MPs with representative deformation histories were selected for detailed analysis (Fig. 7a–c). P1 and P2 are located on the high-speed railway platform, whereas P3 lies on the bare concrete deck. The displacement series of P1 is positively correlated with the structural temperature of the bridge, while P2 exhibits a strong negative correlation. Both platform points are underlain by a concrete-filled steel-tube primary frame that is thermally stable, but are covered by a thin steel roof that is highly sensitive to temperature. Consequently, the temperature change induces a wavy, non-uniform deformation of the roof sheet, as sketched in Fig. 7e. P3, founded on concrete pavement, is almost immune to thermal variations; its deformation trace is therefore flat, with a total range of less than 2 mm.

The longitudinal thermal-deformation rate along the bridge is shown in Fig. 8. Rates vary between −0.09 mm/ ℃ and +0.11 mm/ ℃. Piers #3 and #32 are equipped with fixed pot bearings (restrained in the horizontal plane and stiff in the vertical direction), while pier #12 carries a unidirectional movable bearing (free to translate transversely). These three piers provide high

This contribution has been peer-reviewed. The double-blind peer-review was conducted on the basis of the full paper.
https://doi.org/10.5194/isprs-annals-XI-3-2026-455-2026 | © Author(s) 2026. CC BY 4.0 License.

longitudinal stiffness, so the deck may be regarded as moment-connected to them. Consistently, the longitudinal thermal-deformation rates at piers #3, #12 and #32 are virtually zero (red boxes in Fig. 8). Deck segments on either side of a fixed pier deform in opposite directions: west of the fixed support the deck expands westward, whereas east of the support it expands eastward, as indicated by the red and blue arrows.

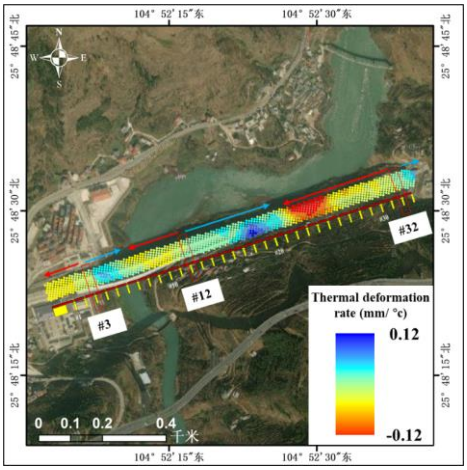

Fig 8. Longitudinal Thermal Deformation Rate along the Bridge

4.3 Two-Dimensional Deformation

Vertical and longitudinal cumulative deformations of the Hutiaohe Bridge were presented in Fig. 9. During the two-year monitoring period, the largest vertical settlement of the bridge is about 4.3 mm, occurred at pier #17—approximately the bridge mid-span. This magnitude is considered normal: the bridge was opened on 28 December 2016 and was still in the slow post-construction settlement phase, subsiding at ≤ 0.5 mm per month. Settlements at piers #3 and #32 were noticeably smaller (Fig. 9b), presumably because these piers are equipped with fixed pot bearings that provide additional vertical restraint.

Longitudinal deformation is illustrated in Figs 9(c) and 9(e); positive values denote eastward displacement and negative values westward. The maximum eastward cumulative movement, +2.48 mm, occurred at pier #7, whereas the largest westward movement, –2.54 mm, was observed at pier #24. According to the Chinese Code for Design of High-Speed Railway (TB 10621-2014), the permissible vertical deflection for ballast-less bridges is 10 mm when the span is < 50 m, and L/5 000 or 20 mm (whichever is smaller) when the span exceeds 50 m. All vertical deformations recorded during the monitoring period lie within these limits, indicating that the bridge is in a satisfactory structural condition.

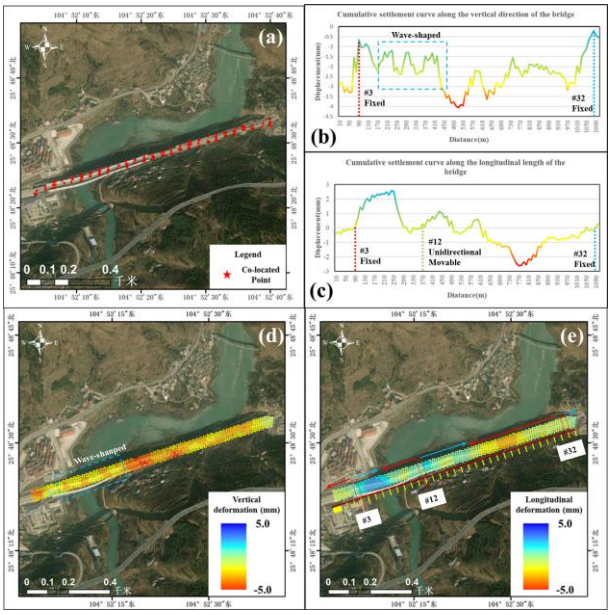

Fig 9. 2-D deformation inversion ensemble: (a) co-located point distribution; (b)& (c) cumulative vertical and longitudinal deformation along the bridge longitudinal section; (d) cumulative vertical settlement; (e) cumulative longitudinal settlement

4.4 FEM

The FEM was employed to simulate the longitudinal deformation of the bridge when the structural temperature rose from 0.4 ℃ to 33.9 ℃. The results are displayed in Fig. 10: panel (a) shows the thermal-deformation rate derived from the InSAR time-series, whereas panel (b) gives the deformation predicted by the FEM under the same 0.4–33.9 ℃ temperature increment. The temperature increase produced systematic thermal movements around piers #3, #12 and #32 (Fig. 10b). West of each fixed pier the deck displaced westward, while east of each pier it displaced eastward—exactly matching the directions retrieved from InSAR. The largest positive displacement (+0.0034 m) occurred at pier #18, and the largest negative displacement (−0.0034 m) at pier #24; these equal-and-opposite values reproduce the antisymmetric pattern seen in the InSAR-derived thermal-deformation-rate map.

Assuming a uniform temperature rise of 33.5℃ (0.4~33.9℃), the longitudinal thermal-deformation rates yield maximum absolute displacements of ≈ 0.0030 m at pier #18 and ≈ 0.0037 m at pier #24, in full agreement with both the magnitude and direction of the FEM predictions (±0.0034 m). The close match between the InSAR observations and the finite-element simulations validates the reliability of both data sets.

This contribution has been peer-reviewed. The double-blind peer-review was conducted on the basis of the full paper.
https://doi.org/10.5194/isprs-annals-XI-3-2026-455-2026 | © Author(s) 2026. CC BY 4.0 License.

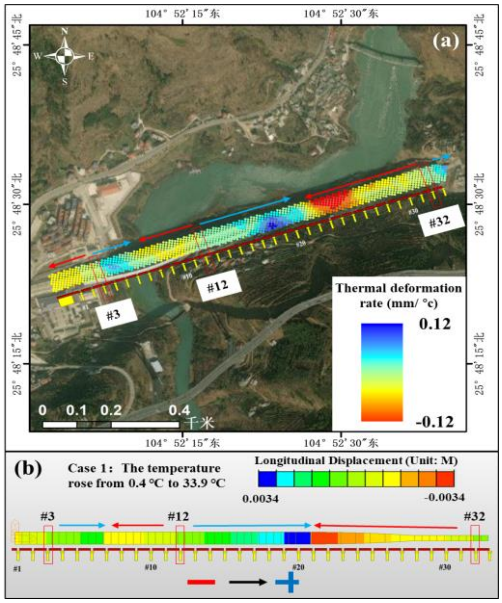

Fig 10. Longitudinal thermal deformation rate of The Bridge: (a) InSAR results; (b) FEM results

5. Conclusions

Based on 64 ascending and descending Sentinel-1 images (2017–2020) and the NOAA global daily meteorological dataset (1929–2024), this study conducted a comprehensive investigation of the Hutiaohe railway bridge in Guizhou by integrating E-PS-InSAR, ANUSPLIN interpolation and FEM.

The bridge exhibits very small deformation rates (≤ 3 mm a^{-1}) and remains globally stable, attributable to the high-grade materials and simply-supported girder configuration adopted for railway bridges. The estimated thermal deformation rate ranges from −0.09 mm/ ℃ to +0.11 mm/ ℃, and different parts of the bridge display distinct thermally induced deformation patterns. The spatial pattern of longitudinal deformations closely matches the temperature-effect distribution, indicating that temperature variation is the primary driver of longitudinal displacement. The InSAR derived thermal-deformation rate agree perfectly with the FEM prediction under the same temperature increment, and the spatial patterns are highly consistent.

Overall, the proposed framework demonstrates strong potential for precise deformation monitoring and condition assessment of railway bridges, offering an effective tool for bridge-health diagnostics.

ACKNOWLEDGEMENTS

This work was supported by the National Key Research and Development Program of China (Grant No. 2023YFC3807500), the Shenzhen Science and Technology Program (Grant No. KCXFZ20230731092803006) and the National Natural Science Foundation of China (Grant No. 42474021).

REFERENCES

Alani, A. M., Tosti, F., Bianchini Ciampoli, L., et al. 2020. An integrated investigative approach in health monitoring of masonry arch bridges using GPR and InSAR technologies. *NDT & E International*, 115: 102288.

Cai, J., Liu, G., Jia, H., Zhang, B., Wu, R., Fu, Y., ... & Zhang, R. 2022. A new algorithm for landslide dynamic monitoring with high temporal resolution by Kalman filter integration of multi-platform time-series InSAR processing. *International Journal of Applied Earth Observation and Geoinformation*, 110, 102812.

Liao, M., Wang, R., Yang, M., Wang, N., Qin, X. 2020. Techniques and applications of spaceborne time-series InSAR in urban dynamic monitoring. *Journal of Radars*, 9(3): 409–424.

Qin, X., Li, Q., Ding, X., Xie, L., Wang, C., Liao, M., ... & Xiong, S. 2021. A structure knowledge-synthetic aperture radar interferometry integration method for high-precision deformation monitoring and risk identification of sea-crossing bridges. *International Journal of Applied Earth Observation and Geoinformation*, 103, 102476.

Schlögl, M., Widhalm, B., Avian, M. 2021. Comprehensive time-series analysis of bridge deformation using differential satellite radar interferometry based on Sentinel-1. *ISPRS Journal of Photogrammetry and Remote Sensing*, 172: 132–146. doi:10.1016/j.isprsjprs. 2020.12.001.

Selvakumaran, S., et al. 2020. Combined InSAR and terrestrial structural monitoring of bridges. *IEEE Transactions on Geoscience and Remote Sensing*, 58(10): 7141–7153.

Shi, M., Chen, B., Gong, H., et al. 2019. Monitoring differential subsidence along the Beijing–Tianjin intercity railway with multiband SAR data. *International Journal of Environmental Research and Public Health*, 16(22): 4453.

Su, Y., Yuan, L., Dong, L., et al. 2022. Development of non-contact detection technology for railway bridges. *Railway Engineering*, 62(01): 11–17.

Wang, L., Zhang, Q., & Li, M. (2024). Correlation Analysis Between Surface Deformation and Internal Structural Stress of Railway Bridges Based on InSAR and FEM Data Fusion. *Remote Sensing*, 16(3), 589. https://doi.org/10.3390/rs16030589

Xiao, B., Zhao, J., Li, D., et al. 2022. The monitoring and analysis of land subsidence in Kunming (China) supported by time series InSAR. *Sustainability*, 14(19): 12387.

Xiong, S., Wang, C., Qin, X., et al. 2021. Time-series analysis on persistent scatter-interferometric synthetic aperture radar (PS-InSAR) derived displacements of the Hong Kong–Zhuhai–Macao Bridge (HZMB) from Sentinel-1A observations. *Remote Sensing*, 13(4): 546. doi:10.3390/rs13040546.

Zhang, H., Liu, J., & Chen, F. 2023. Integration of InSAR Data and Finite Element Model Simulation for Structural Health Monitoring of Long-Span Railway Bridges. *Journal of Bridge Engineering*, 28(7), 04023056. doi.org/10.1061/(ASCE)BE.1943-5592.0002189